

Bayesian Nonparametric Poisson-Process Allocation for Time-Sequence Modeling

Hongyi Ding¹

hongyi@ms.k.u-tokyo.ac.jp

Mohammad Emtyaz Khan²

emtyaz.khan@riken.jp

Issei Sato¹

sato@k.u-tokyo.ac.jp

Masashi Sugiyama^{1,2}

sugi@k.u-tokyo.ac.jp

¹The University of Tokyo, Japan

²RIKEN

Abstract

Analyzing the underlying structure of multiple time-sequences provides insight into the understanding of social networks and human activities. In this work, we present the *Bayesian nonparametric Poisson process allocation* (BaNPPA), a generative model to automatically infer the number of latent functions in temporal data. We model the intensity of each sequence as an infinite mixture of latent functions, each of which is the square of a function drawn from a Gaussian process. A technical challenge for the inference of such mixture models is the *identifiability* issue between coefficients and the scale of latent functions. We propose to cope with the identifiability issue by regulating the volume of each latent function and derive a variational inference algorithm that can scale well to large-scale data sets. Our algorithm is computationally efficient and scalable to large-scale datasets. Finally, we demonstrate the usefulness of the proposed Bayesian nonparametric model through experiments on both synthetic and real-world data sets.

1 Introduction

The Internet age has made it possible to collect a huge amount of temporal data available in the form of time-sequences. Each time-sequence consists of timestamps which record the arrival time of events, e.g., postings of tweets on Twitter or announcements of life events on Facebook. In real-world problems arising in areas such as social science (Gao et al., 2015),

health care (Lian et al., 2015) and crime prevention (Liu and Brown, 2003), time-sequence modeling is extremely useful since it can help us predict future events and understand the reasons behind them.

When modeling a collection of time-sequences, a key idea is “to separate the data set into clusters, and yet allow the groups to remain linked to share statistical strength” (Teh et al., 2005). Several models have been proposed on the basis of this simple idea, e.g., the convolution process (Gunter et al., 2014), nonnegative matrix factorization (NMF) (Miller et al., 2014), and latent Poisson process allocation (LPPA) (Lloyd et al., 2016). These models employ latent factors to share statistical strength and combine them to model the correlation within and among time-sequences.

Among these models, LPPA is a powerful approach since it uses a set of latent functions, each of which is the square of a random function drawn from a Gaussian process (GP). Such continuous latent functions do not require the careful discretization unlike those in NMF, and are able to flexibly model complex structures present in data.

A limitation of LPPA is the model selection issue, since the number of latent functions needs to be set beforehand. If this number is much larger than the actual number of latent functions required to explain the data, LPPA will use all latent functions. There is no mechanism in LPPA to prevent this spread of information over a large number of latent functions. This creates a problem for time-sequence modeling especially when our goal is to understand the real reasons behind the events. For example, it might be difficult to explain the retweet patterns in Twitter with LPPA, since a sudden avalanche of retweets is quite common (Gao et al., 2015) and LPPA will use all its latent functions to explain these spiky patterns.

The above problem can be solved by using Bayesian nonparametric (BNP) methods, with which the model can automatically determine the number of relevant latent functions. However, as we argue in this pa-

per, a direct application of existing BNP methods is challenging for LPPA. An obvious issue is that using hierarchical models typically requires the use of MCMC algorithms which are usually slow to converge for large data sets. A more essential and technically intricate issue is that a naive application of BNP methods in LPPA suffer *unidentifiability* because the GP-modulated latent functions are not normalized. Unidentifiability is bad news when our focus is to understand the reasons behind the events.

In this paper, we propose a new model and derive its learning algorithm to solve these problems. Our model, which we call the *Bayesian nonparametric Poisson process allocation* (BaNPPA) model, enables automatic inference of the number of latent functions while retaining accuracy, interpretability, and scalability of LPPA. Unlike hierarchical models (Teh et al., 2005) which promote sharing through the common base measure, latent functions in our model are shared across all time-sequences due to the size-biased ordering which promotes sharing by penalizing latent functions that belong to higher indices (Gopalan et al., 2014; Pitman et al., 2015). The size-biased ordering restricts the use of all latent functions while affording scalable inference algorithms.

We derive a scalable variational inference algorithm for BaNPPA and solve the identifiability issue by adding a constraint within the inference algorithm to regulate the volume of each latent function. Overall, we present a scalable and accurate Bayesian nonparametric approach to time-sequence modeling.

2 Time-Sequence Modeling and Its Challenges

We start with a brief description of existing models for time-sequences. Throughout the paper, we denote the set of time-sequences by Y which consists of D individual time-sequences. Each time-sequence contains a set of time-stamps recording the arrival time of events. We denote a time-sequence $\mathbf{y}_d = \{t_n^d \in \mathcal{T}\}_{n=1}^{N_d}$ where $\mathcal{T} \subset \mathbb{R}^+$ is a specified time window within which events occur and N_d is the number of events in the d 'th sequence. Our focus in this paper is to develop flexible models for such time-sequences.

To model each time-sequence, a common approach is to use the temporal Cox process (Adams et al., 2009; Lloyd et al., 2015). A temporal Cox process is defined via a stochastic intensity function $\lambda(t) : \mathbb{R}^+ \rightarrow \mathbb{R}^+$ (Kingman, 1993). Given the intensity function $\lambda(t)$ and a time window $\mathcal{T} \subset \mathbb{R}^+$, the number of events $N(\mathcal{T})$ is Poisson distributed with the rate parameter $\int_{\mathcal{T}} \lambda(s)ds$ and the likelihood of observed sequence

$\{t_n\}_{n=1}^{\tilde{N}}$ drawn from the temporal Cox process is

$$P(\{t_n\}_{n=1}^{\tilde{N}} | \lambda(t)) = \exp\left(-\int_{\mathcal{T}} \lambda(s)ds\right) \prod_{n=1}^{\tilde{N}} \lambda(t_n). \quad (1)$$

In LPPA, to model multiple time-sequences, the d 'th time-sequence is assumed to be generated by a temporal Cox process with the intensity function $\lambda_d(t)$. The intensity function $\lambda_d(t)$ is modeled using a linear combination of K latent functions as below:

$$\lambda_d(t) = \sum_{k=1}^K \theta_{dk} f_k^2(t), \quad \theta_{dk} \geq 0, \quad (2)$$

where $f_k(t)$ is a function drawn from a GP prior and θ_{dk} is its weight for the d 'th sequence. To ensure the non-negativity of λ_d , the latent function is the square of the function f_k and θ_{dk} is assumed to be non-negative.

LPPA uses a GP prior to independently draw functions $f_k(t)$, which enables the modeling of intensity functions with a complex shape. Each weight θ_{dk} is assumed to be deterministic. Both $\{f_k(t)\}$ and $\{\theta_{dk}\}$ are estimated using a variational-inference procedure of Titsias (2009) that uses sparse GPs. This enables scalable inference with the computational complexity $O(KNM^2)$, where K is the number of basis functions, N is the total number of events in Y , and M is the number of pseudo inputs in sparse GPs.

The number of latent functions K is a hyper-parameter that needs to be set beforehand. Besides computational issues in setting this number, this poses a serious issue when the model is used to understand the reasons behind observed sequences. The GP prior gives LPPA the flexibility to model complex shapes, but when K is much larger than what it needs to be, each latent function $f_k^2(t)$ is assigned a non-zero weight θ_{dk} for some d . Basically, the model ends up using all latent functions, which spoils the interpretability completely. We give empirical evidence in support of this claim and correct this behavior by using a BNP method.

A direct application of existing BNP methods might come with a cost of increased computation time and a loss of the flexibility in latent functions. The problem lies in the limited choice of latent functions, each of which is assumed to be a *normalized density function* with a volume¹ equal to 1. Specifically, previous studies (Kottas, 2006; Ihler and Smyth, 2007) model the intensity function of a time-sequence using a Dirichlet process mixture of parametric *normalized density functions*. We show an example below of such a model

¹The volume of a function $f(t), t \in \mathcal{T}$ is defined as the integral $\int_{\mathcal{T}} f(t)dt$.

with $K = \infty$,

$$\lambda_d(t) = s_d \sum_{k=1}^{\infty} \theta_{dk} \tilde{f}(t; \psi_k), \quad (3)$$

where each latent function $\tilde{f}(t; \psi_k)$ is a *normalized density function* with parameter ψ_k and the weights also sum to one $\sum_{k=1}^{\infty} \theta_{dk} = 1$ ($s_d > 0$ is the rate parameter that models the number of events $N(\mathcal{T})$). $\tilde{f}(t; \psi_k)$ is chosen to be the beta distribution in Kottas (2006) and the truncated Gaussian distribution in Ihler and Smyth (2007). This type of models require MCMC sampling algorithms which could be slow for large data sets and the parametric form limits the flexibility of each latent function. To the best of our knowledge, it is still unclear how to build a nonparametric prior for the *normalized density functions* while enabling scalable inference, e.g., via variational methods.

3 Proposed Model

We build BaNPPA upon LPPA. We combine the GP-modulated latent functions and the mixture structure shown in Equation (3). With the former, we can enjoy both the flexibility of the latent function and the computational efficiency, while we use the latter to automatically determine the number of latent functions. We do so by first moving the normalization requirement from the model to the inference procedure.

Specifically, we use a GP prior for f_k and let $\tilde{f}(t; \psi_k) = f_k^2(t)$ in Equation (3) to get the following model:

$$\lambda_d(t) = s_d \sum_{k=1}^{\infty} \theta_{dk} f_k^2(t), \quad (4)$$

where both s_d and θ_{dk} are non-negative, and $\sum_{k=1}^{\infty} \theta_{dk} = 1$. The latent functions $\{f_k^2\}$ are unnormalized. This creates an unidentifiable model as we explain later in Section 4.

We denote a Gaussian process by $\text{GP}(m(t), \kappa(t, t'))$ with mean function m and covariance function κ , and a Poisson process as PP. We set $m_k(t) \equiv g$ and g is a positive scalar for simplicity and use the automatic relevance determination (ARD) covariance function. The generative process of our model is shown below.

1. Draw $f_k \sim \text{GP}(m_k(t), \kappa_k(t, t'))$ for $k = 1, \dots, \infty$.
2. For each sequence $d = 1, \dots, D$,
 - Draw $\theta'_{dk} \sim \text{Beta}(1, \alpha)$ for $k = 1, \dots, \infty$.
 - Calculate $\theta_{dk} = \theta'_{dk} \prod_{l=1}^{k-1} (1 - \theta'_{dl})$.
 - Draw $s_d \sim \text{Gamma}(a_0, b_0)$.
 - Draw the points $\mathbf{y}_d \sim \text{PP}(s_d \sum_{k=1}^{\infty} \theta_{dk} f_k^2(t))$.

The above model uses a stick-breaking process which enables the size-biased ordering (Pitman et al., 2015) to automatically determine the number of latent functions. Both the latent functions $\{f_k^2(t)\}$ and the weights $\{\theta_{dk}\}$ use the same set of indices $k = 1, \dots, \infty$. This implies that when generating the d 'th time-sequence, the latent function at a lower index k is more likely to be assigned a larger weight θ_{dk} . In this way, all time-sequences share the same set of latent functions. The size-biased ordering affords scalable inference algorithms (Gopalan et al., 2014) which is why we use this structure rather than a hierarchical one.

In this model, we need to guarantee that the expected intensity function at any time $\mathbb{E}[\lambda_d(t)]$ is finite. This can be achieved by fixing the parameter g of the mean function $m_k(t)$ and the hyper-parameters $\{\gamma_k\}$ of ARD covariance functions $\kappa_k(t, t') = \gamma_k \exp(-(t - t')^2/(2a_k^2))$ in advance. When these hyper-parameters are fixed, the value of $\mathbb{E}[\lambda_d(t)]$ is bounded since

$$\begin{aligned} \mathbb{E}[\lambda_d(t)] &= \mathbb{E}[s_d \sum_{k=1}^{\infty} \theta_{dk} f_k^2(t)] \leq \mathbb{E}[s_d] \max_k \mathbb{E}[f_k^2(t)] \\ &= \frac{a_0}{b_0} \max_k \left(\mathbb{E}^2[f_k(t)] + \text{var}[f_k(t)] \right). \end{aligned} \quad (5)$$

4 Identifiability Problem

The model in Equation (4) relaxes the normalization requirement in the model of Equation (3). However, this gives rise to an additional identifiability problem because the volume of each latent function is not regulated. The identifiability problem is that $\forall \epsilon_k > 0$, $k = 1, \dots, \infty$, the following combination $(s'_d, \{\theta'_{dk}\}, \{f'_k\})$ gives the same intensity function $\lambda_d(t)$, where $\bar{\epsilon}_d = \sum_{v=1}^{\infty} \theta_{dv} \epsilon_v$:

$$(s'_d, \{\theta'_{dk}\}, \{f'_k\}) \triangleq \left(s_d \bar{\epsilon}_d, \left\{ \frac{\theta_{dk} \epsilon_k}{\bar{\epsilon}_d} \right\}, \left\{ \frac{f_k}{\sqrt{\epsilon_k}} \right\} \right). \quad (6)$$

This may bring harm to our model. In mixture modeling, we are implicitly allocating points in Y to each latent function. However, in the current model, each latent function $f_k^2(t)$ is sensitive to the allocation behavior in the sense that when being allocated with more points, the volume of the latent function $\int_{\mathcal{T}} f_k^2(t) dt$ will get larger. This adds more shrinkage to the mixture model and the model tends to over-shrink the latent functions. Moreover, this un-identifiability is problematic when we want to adjust the hyper-parameter α in the beta prior to achieve a certain degree of shrinkage. Therefore, we need to regulate the volume of each latent function. An alleviation solution based on the variational inference is provided in Section 5.2.

There is also another common identifiability problem in such mixture models. It is the identifiability of each

latent function. Lloyd et al. (2016) claimed that LPPA is non-identifiable and non-unique since there may be multiple decompositions that are well supported by the data. In BaNPPA, since we use the size-biased ordering, the model tends to sort the latent functions and the non-identifiability of solutions is mitigated.

5 Inference

In this section, we first provide the general variational inference framework and give an alleviation solution in Section 5.2. The derivation of the evidence lower bound (ELBO) and its derivatives is provided in the supplementary material.

5.1 Variational Inference

Let $Y = \{\mathbf{y}_d\}$, $\mathbf{s} = \{s_d\}$, $\Theta = \{\theta_{dk}\}$, $\mathbf{f} = \{f_k\}$ and $\mathbf{H} = \{\kappa_k\}$. The joint distribution over the variables can be expressed as

$$\begin{aligned} p(Y, \Theta, \mathbf{s}, \mathbf{f}) &= \prod_{k=1}^{\infty} p(f_k; g, \kappa_k) \prod_{d=1}^D p(s_d; a_0, b_0) \\ &\times \prod_{d=1}^D \prod_{k=1}^{\infty} p(\theta_{dk}; \alpha) \prod_{d=1}^D p(\mathbf{y}_d | \mathbf{f}, \theta_d, s_d). \end{aligned}$$

We follow Blei et al. (2006) and truncate the number of latent functions to K . K is usually selected to be larger than the expected number of latent functions used by the data. Then the model will automatically shrink additional latent functions. We use the same set of pseudo inputs $\{t_m\}_{m=1}^M$, $M < N$ for each f_k so that the evaluations of all latent functions share the same level of accuracy (Lloyd et al., 2016).

Let $\mathbf{f}_{k,M} \triangleq [f_k(t_1), \dots, f_k(t_M)]^\top$, $\kappa_{k,MM}$ be the covariance matrix for pseudo inputs in which $\kappa_{k,MM}[i, j] = \kappa_k(t_i, t_j)$ and $\mathbf{g}_M \in \mathbb{R}^M$ be the vector with all elements equal to g . The variational distributions are given as follows:

$$\begin{aligned} q(s_d) &= \delta_{\eta_d}, \\ q(\theta'_{dk}) &= \mathbb{I}(k < K) \text{Gamma}(\tau_{dk,0}, \tau_{dk,1}) \\ &+ \mathbb{I}(k = K) \delta_1 + \mathbb{I}(k > K) p(\theta'_{dk}), \\ q(\mathbf{f}_{k,M}) &= \mathbb{I}(k \leq K) \mathcal{N}(\boldsymbol{\mu}_k, \Sigma_k) \\ &+ \mathbb{I}(k > K) \mathcal{N}(\mathbf{g}_M, \kappa_{k,MM}), \end{aligned}$$

where $\mathbb{I}(\cdot)$ is the indicator function. Then the variational distribution $q(Y, \Theta, \mathbf{s}, \mathbf{f})$ is

$$\prod_{k=1}^{\infty} p(\mathbf{f}_{k,N} | \mathbf{f}_{k,M}) q(\mathbf{f}_{k,M}) \prod_{d=1}^D q(s_d) \prod_{d=1}^D \prod_{k=1}^{\infty} q(\theta_{dk}).$$

We use the true $p(\mathbf{f}_{k,N} | \mathbf{f}_{k,M})$ as in Titsias (2009). Following Lian et al. (2015), we use the re-

parametrization $\Sigma_k = L_k L_k^T$ by Cholesky decomposition and add positivity constraints on the diagonal elements in L_k , without which the value $\log |\Sigma_k|$ in the Kullback-Leibler divergence may be unstable. We use the delta function as the variational distribution for \mathbf{s} and in this case we obtain a MAP estimate.

Let $\boldsymbol{\tau} = \{(\tau_{dk,0}, \tau_{dk,1})\}$, $\mathbf{L} = \{L_k\}$ and $\boldsymbol{\eta} = \{\eta_d\}$. We could maximize the ELBO using coordinate ascent with respect to the parameters $\Phi = \{\boldsymbol{\eta}, \boldsymbol{\tau}, \boldsymbol{\mu}, \mathbf{L}, \mathbf{H}, a_0, b_0, \alpha\}$ within the variational expectation-maximization framework.

5.2 An Alleviation Solution to the Identifiability Problem

So far, the framework seems very traditional. However, as we mentioned in Section 3, this weak model has an additional identifiability problem which may over-shrink the components.

Directly putting a constraint on the volume of the latent functions $\int_{\mathcal{T}} f_k^2(t) dt$, where f_k is drawn from the posterior process $p(f_k | Y)$, is not applicable, since it will make the inference intractable. In order to obtain a tractable constraint, we require that on average each function f_k drawn from the posterior process approximately satisfies the integral constraint, which is

$$\iint_{\mathcal{T}} p(f_k | Y) f_k^2(s) ds df_k = A, \quad k = 1, \dots, K, \quad (7)$$

where A is a positive constant. Within the variational inference framework, we use the variational distribution $q(f_k)$ to approximate the posterior $p(f_k | Y)$. Thus we can add the following constraint to each latent function:

$$\iint_{\mathcal{T}} q(f_k) f_k^2(s) ds df_k = A, \quad k = 1, \dots, K. \quad (8)$$

5.3 Optimization with Equality Constraints

Given the equality constraints in Equation (8), the optimization process can be formulated as follows, where we denote the ELBO as $\mathcal{L}_1(\Phi)$:

$$\max_{\Phi} \mathcal{L}_1(\Phi), \quad \text{s.t. } h_k(\Phi) = 0, \quad k = 1, \dots, K, \quad (9)$$

$$h_k(\Phi) = \int_{\mathcal{T}} \mathbb{E}_q[f_k^2(s)] ds - A.$$

Problem (9) is an optimization problem with equality constraints and we use the augmented Lagrangian method (Bertsekas, 2014) to solve this problem. Then Problem (9) is reduced to a series of related optimization problems

$$\max_{\Phi} \mathcal{L}_1(\Phi) - \sum_{k=1}^K \left(w_{ik} h_k(\Phi) + \frac{1}{2} v_{ik} h_k^2(\Phi) \right), \quad (10)$$

Table 1: Data sets used for experiments.

Data set	D	N _{train}	N _{test}	\mathcal{T}
Synthetic A	200	6,304	6,010	[0,60]
Synthetic B	250	8,074	8,110	[0,80]
Microblog	500	44,628	44,352	[3,15]
Citation	600	106,113	106,340	[0,20]

where $i \in \mathbb{N}^+$, $0 < v_{ik} \leq v_{i(k+1)}$ and $\{w_{ik}\}$ are bounded. We denote this objective by $L_{\mathbf{v}_i}(\Phi, \mathbf{w}_i)$. For each optimization problem in Equation (10), $L_{\mathbf{v}_i}(\Phi, \mathbf{w}_i)$ is still upper bounded and a brief proof can be found in the supplementary material. Thus if we use coordinate ascent with respect to parameters in Φ , the algorithm is guaranteed to arrive at a local maximum.

5.4 Computational Complexity

After adding the constraint, each optimization problem in Equation (10) does not become significantly more expensive. Although in Equation (10), we have to optimize additional parameters $\{\boldsymbol{\eta}, \boldsymbol{\tau}\}$ in Φ , the bottleneck is still the matrix-matrix multiplication in the evaluation of $q(\mathbf{f}_{k,N})$. For one iteration of the training procedure, the computational complexity is $\mathcal{O}(KNM^2)$, which is the same as LPPA.

Since there are potentially infinitely many optimization problems to be solved, one might expect the total computational complexity is worse than LPPA. We alleviate this issue by following the suggestions in the augmented Lagrangian method (Bertsekas, 2014). Namely, we reuse the final value Φ_{i-1} of the previous optimization as the starting value for the i -th round and terminate the training process when the relative change in the likelihood is small. From experiments, we could observe that the convergence of BaNPPA is rather fast and comparable to LPPA.

6 Experiments

We evaluate our proposed Bayesian nonparametric model BaNPPA and compare it with latent Poisson process allocation (LPPA). We also test BaNPPA with no constraints (BaNPPA-NC).

We test three algorithms on two synthetic data sets and two real-world data sets. For each sequence in the data set Y , we divide it into two halves by allocating each event into either half with probability 0.5. One half is used for training and the other is for testing.

See Table 1 for detailed information, where D , N_{train} , N_{test} and \mathcal{T} are the number of sequences, the total

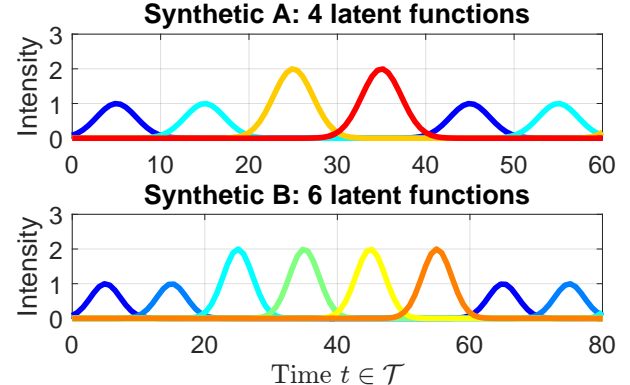


Figure 1: **Synthetic data sets**. Illustration about the latent functions. Row 1: Four latent functions. Row 2: Six latent functions. In both data sets, two of the latent functions have two peaks while the rest have one peak.

number of events in the training set Y_{train} , the total number of events in the testing set Y_{test} and the time window respectively.

1) Synthetic A data set. We sample 200 time-sequences from $\lambda_d(t) = s_d \sum_{k=1}^4 \theta_{dk} \bar{f}(t; \psi_k)$, where $\boldsymbol{\theta}_d \sim \text{Dir}(1.2, 1, 0.8, 0.6)$ and $s_d \sim \text{Gamma}(2, 3)$.

2) Synthetic B data set. We sample 250 time-sequences from $\lambda_d(t) = s_d \sum_{k=1}^6 \theta_{dk} \bar{f}(t; \psi_k)$, where $\boldsymbol{\theta}_d \sim \text{Dir}(1.2, 1, 0.8, 0.6, 0.5, 0.5)$ and $s_d \sim \text{Gamma}(2, 3)$.

$\text{Dir}(\cdot)$ denotes the Dirichlet distribution. Latent functions $\bar{f}(t; \psi_k)$ for the Synthetic A data set and the Synthetic B data set are plotted in Figure 1. Details on the data generation process can be found in the supplementary material.

3) Microblog data set. We download 500 tweets and all retweets of each tweet from 7 tweet-posters on Sina micro-blog platform through official API². There are many reasons which could cause a different retweet pattern. One reason is that tweets posted at an inactive hour will regain the attention from the followers several hours later next morning (Gao et al., 2015). Two examples are given in Figure 2. But it is hard to find all the reasons and determine the number of retweet patterns beforehand.

4) Citation data set. We obtain the Microsoft academic graph before February 5th, 2016 from KDDcup 2016³. The original data set contains 126,909,021 papers and we use a subset. We study the pattern of citations within 20 years after a paper is published.

²<http://open.weibo.com/wiki/Oauth/en>

³<https://kddcup2016.azurewebsites.net/>

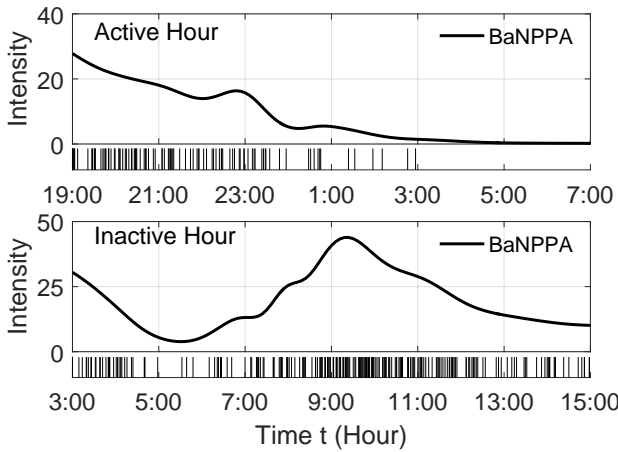


Figure 2: **Microblog data set.** Illustrations of different retweet patterns. Top: A tweet posted in an active hour. Bottom: A tweet posted in an inactive hour. Smooth lines are the mean intensity functions inferred from BaNPPA. Small bars at the bottom are the timestamps of each retweet.

An observation about the pattern is that some papers quickly get citations while some others get citations very slowly. We only consider papers which were published more than 20 years before. Two examples are given in the supplementary material.

Evaluation Metrics. We evaluate the model in terms of two metrics.

a) To measure the predictive performance, we follow Lloyd et al. (2015) and use the test likelihood $\mathcal{L}_{\text{test}}$.

$$\begin{aligned} \mathcal{L}_{\text{test}} &\triangleq \sum_{d=1}^D \sum_{n=1}^{N_d^{\text{test}}} \ln \left(s_d \sum_{k=1}^K \theta_{dk} \exp \left(\mathbb{E}_q[\ln f_k^2(t_n^d)] \right) \right) \\ &\quad - \sum_{d=1}^D s_d \sum_{k=1}^K \theta_{dk} \int_{\mathcal{T}} \mathbb{E}_q[f_k^2(s)] ds. \end{aligned} \quad (11)$$

$\mathcal{L}_{\text{test}}$ can be seen as a lower bound of the true test likelihood $\ln p(Y_{\text{test}}|Y_{\text{train}})$. For LPPA, the allocation parameters θ_{dk} are the point-estimated weights and the rate parameter $s_d = 1$. For BaNPPA and BaNPPA-NC, we also use $\mathcal{L}_{\text{test}}$ and draw samples of s_d , θ_{dk} from the variational distribution $q(s_d, \theta_d)$. We can use Equation (11) on the training data to obtain a lower bound of the training likelihood $\mathcal{L}_{\text{train}}$. Detailed derivations and explanations are given in the supplementary material.

b) To measure how much each latent function is occupied by the model, we calculate the normalized al-

location matrix $\hat{\Theta} \in \mathbb{R}_+^{D \times K}$, where

$$\hat{\theta}_{dk} = \frac{\mathbb{E}_q[\theta_{dk} \int_{\mathcal{T}} f_k^2(s) ds]}{\sum_{m=1}^K \mathbb{E}_q[\theta_{dm} \int_{\mathcal{T}} f_m^2(s) ds]}. \quad (12)$$

The intuition behind the normalization is that in LPPA and BaNPPA-NC the volume of each latent function $\int_{\mathcal{T}} f_k^2(s) ds$ is not regulated and also contributes to the mixture weight θ_{dk} .

Based on $\hat{\Theta}$, we can calculate the normalized expected responsibility (NER) $\hat{v}_k = \sum_{d=1}^D \hat{\theta}_{dk} / D$, $k = 1, \dots, K$ to measure the expected occupancy of each latent function. A larger NER indicates that the corresponding latent function is more often occupied by the model. We can also calculate the unnormalized expected responsibility (UNER) $v_k = \sum_{d=1}^D \mathbb{E}_q[\theta_{dk}] / D$, $k = 1, \dots, K$ which omits the contribution of the volume.

Experimental settings. We re-implement the LPPA algorithm (Lloyd et al., 2016) and change the number of latent functions. For BaNPPA/BaNPPA-NC, we fix the truncation number to $K = 14$. Since the value of the hyper-parameter α in the stick-breaking process prior is critical in BNP models, we conduct experiments on two different settings of the hyper-parameter α . One is optimizing α and the other is fixing α . In both settings, all experiments are repeated five times.

In the first setting, we initialize $\alpha = 1$ and use the variational expectation-maximization to update α in the training process. The optimization method can be found in the supplementary material. In the second setting, we vary the initial value of α in $[1.1, 2, 4, 6, 8]$ and fix it in the training process.

We use a random initialization for the allocation matrix Θ and τ . For sparse GPs, we use 18, 24, 30 and 30 pseudo inputs for the four data sets, respectively. We follow the common practice and add a jitter term εI to the covariance matrix $\kappa_{k,MM}$ to avoid numerical instability (Bauer et al., 2016). For the augmented Lagrangian method in BaNPPA, we regulate the expected volume of each latent function by $A = N_{\text{train}} / D$. We follow the suggestions from Bertsekas (2014) and use $\mathbf{v}_{i+1} = 4\mathbf{v}_i$, $\mathbf{w}_{i+1} = \mathbf{w}_i + \mathbf{v}_i \mathbf{h}(\Phi_i)$. We initialize $v_{1k} = 4, w_{1k} = 1, \forall k$. For hyper-parameters a_0 and b_0 in the gamma distribution, we fit the gamma distribution to the counts $\{N_d^{\text{train}}\}_{d=1}^D$ and use the results (a'_0, b'_0) to set (a_0, b_0) . Since A is not necessarily equal to 1, we set $a_0 = a'_0$ and $b_0 = A b'_0$.

For LPPA, BaNPPA-NC and each optimization problem in BaNPPA, since there are positivity constraints on \mathbf{L} and τ we use the limited-memory projected quasi-newton algorithm (Schmidt et al., 2009). We terminate the training process when the relative change in ELBO is less than 10^{-3} . For BaNPPA, we stop

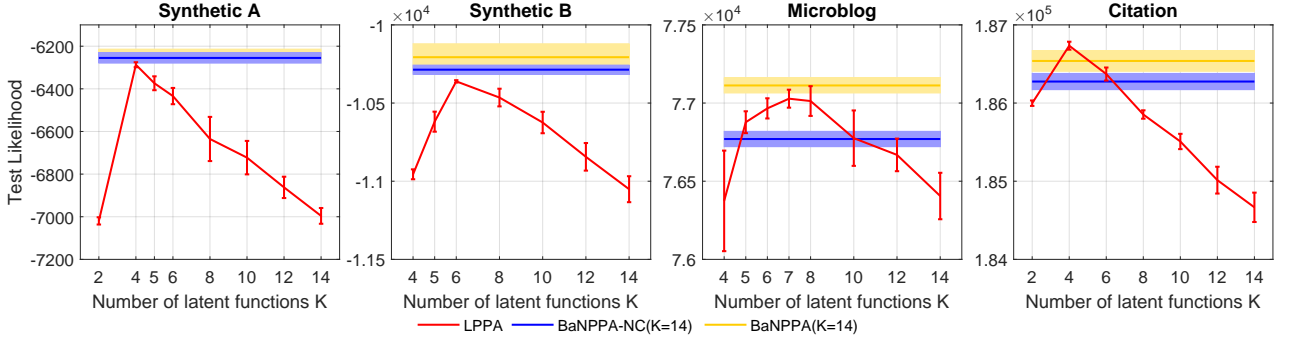


Figure 3: The comparison of the test likelihood among three algorithms. For LPPA, we change the number of latent functions K . For BaNPPA/BaNPPA-NC, we fix $K = 14$ and optimize the hyper-parameter α using variational expectation-maximization. Error bars and shaded areas show the 95% confidence intervals.

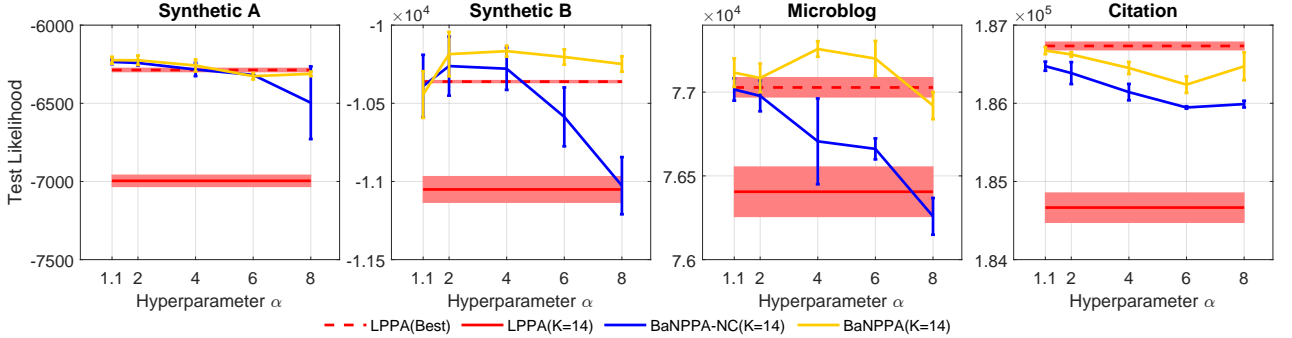


Figure 4: The comparison of the test likelihood for BaNPPA and BaNPPA-NC when fixing hyper-parameter α . For BaNPPA/BaNPPA-NC, we fix $K = 14$ and do not optimize α . The best results and the results when $K = 14$ for LPPA are also given. Error bars and shaded areas show the 95% confidence intervals.

the training process when the relative change between $L_{\mathbf{v}_i}(\Phi_i, \mathbf{w}_i)$ and $L_{\mathbf{v}_{i+1}}(\Phi_{i+1}, \mathbf{w}_{i+1})$ is less than 10^{-3} .

Experimental results. We report the results of two different settings of the hyper-parameter α . The comparison of the test likelihood when optimizing α is given in Figure 3 and the comparison of the train likelihood $\mathcal{L}_{\text{train}}$ is given in the supplementary material. The comparison of the test likelihood when fixing α is given in Figure 4.

We could notice in Figure 3 that for LPPA, the test likelihood drops when we increase the number of latent functions K . BaNPPA achieves similar results with the best results in LPPA on the four data sets.

In Figure 5, we plot the average NER of each latent function during the five trials and the top four latent functions for both LPPA and BaNPPA when optimizing α . The plot of the top four latent functions is based on the result with the best test likelihood in five trials. We can notice that when $K = 14$, LPPA uses all latent functions evenly. We reorder the latent functions according to their corresponding NERs and the result of LPPA can not recover the four true latent

functions in Figure 1. These facts indicate that LPPA tends to over-fit the data when K is large. BaNPPA, however, does not suffer from over-fitting when $K = 14$ and it can automatically shrink additional latent functions. In Figure 5, BaNPPA mainly occupies four latent functions according to the result of NER and has small values of NER on the remaining latent functions.

On the Microblog data set, we plot the normalized allocation matrix $\hat{\Theta}$ in the trial with the best test likelihood. We sample 100 time-sequences from the data set and reorder the ID of the time-sequences: first by the index of the largest element $c_d = \arg \max_k \theta_{dk}$ (e.g., group all time-sequences whose $c_d = 1$ together), and then by the value of the largest element $\max_k \theta_{dk}$. The results for LPPA and BaNPPA are given in Figure 6. We can see that LPPA indeed uses all latent functions to explain the data set, since the elements with large values nearly lie on the diagonal of the matrix. BaNPPA, on the other hand, occupies fewer latent functions with lower indices due to the size-biased ordering. The comparison of the three algorithms on the four data sets can be found in the supplementary material.

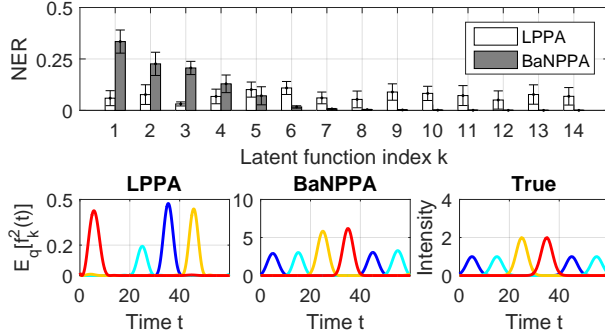


Figure 5: **Synthetic A** data set. Comparisons between LPPA and BaNPPA when optimizing α . (Row 1): NER for each latent function during five trials with error bars showing the 95% confidence intervals. (Row 2): Top four latent functions for LPPA (Left) and BaNPPA (Middle) and true latent functions (Right).

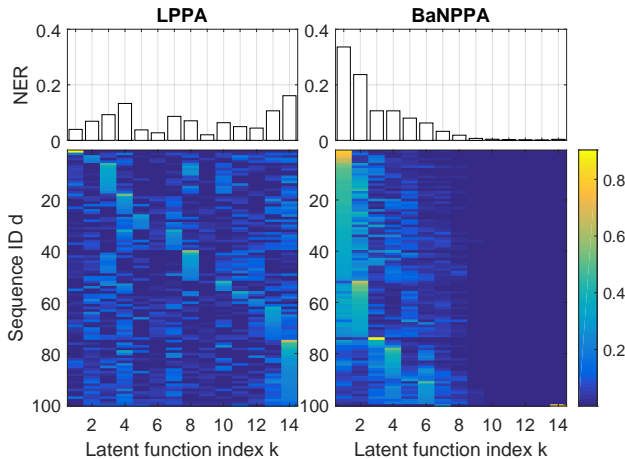


Figure 6: **Microblog** data set. Comparison of the matrix $\hat{\Theta}$ between LPPA (Left) and BaNPPA (Right).

Model identifiability. In Figure 3, we can notice that BaNPPA-NC gets slightly worse on the four data sets than BaNPPA. In Figure 4, when increasing the value of hyper-parameter α , the performance of BaNPPA-NC gets worse on the Synthetic B and Microblog data set and gets slightly worse on the Synthetic A and Citation data set. The performance of BaNPPA stays relatively stable on the four data sets.

To investigate the reason behind this, in Figure 7 we plot the NER and the expected volume $\mathbb{E}_q[\int_T f_k^2(t)dt]$ of each latent function during the five trials on the Synthetic B data set when $K = 14$ and $\alpha = 8$. We can notice that BaNPPA-NC and BaNPPA are comparable in terms of the UNER since UNER is calculated using the mixture weights $\mathbb{E}_q[\theta_{dk}]$, which are influenced by α . The imbalance in UNER at each index k is due to

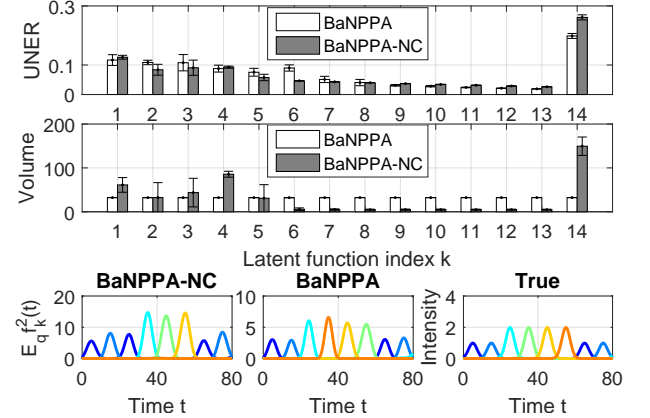


Figure 7: **Synthetic B** data set. Comparisons between BaNPPA and BaNPPA-NC when fixing $\alpha = 8$. (Row 1): UNER for five trials. (Row 2). Expected volumes for each latent function during five trials. Error bars show the 95% confidence intervals. (Row 3): Top six latent functions for BaNPPA-NC (Left) and BaNPPA (Middle) and true latent functions (Right).

the usage of truncated Dirichlet Processes. However, in BaNPPA-NC the volume of each latent function is not regulated and the latent function with a larger $\mathbb{E}_q[\sum_d \theta_{dk}]$ has a larger expected volume. The variety in the volume adds more shrinkage to BaNPPA-NC. As a result, BaNPPA-NC merges two true latent functions. BaNPPA, on the other hand, has almost the same expected volume for each latent function and recovers true latent functions.

Overall, BaNPPA-NC performs similarly to BaNPPA when the latent structure is simple but becomes less favorable when the structure gets complicated. We add three additional synthetic data experiments in which the actual K is large in the supplementary material.

7 Conclusions and Future Work

We considered the task of automatically inferring the number of latent functions for multiple time-sequences. We have proposed the model called BaNPPA, in which we applied the BNP methods to the framework of LPPA and imposed an equality constraint on the variational distribution of the Gaussian process to regulate the volume of each latent function. For future work, we are considering adopting the stochastic optimization for Gaussian processes (Hensman et al., 2013) to handle large data sets and further speed up the training process. Besides, how to combine the volume constraint and the Gaussian process prior would also be an interesting and challenging problem.

Acknowledgements

MS acknowledges support by KAKENHI 17H00757.

A Evidence Lower Bound $\mathcal{L}_1(q)$

Using Jensen's inequality, we bound the marginal log likelihood of the observed sequence $\{\mathbf{y}_d\}$. Hereafter we omit hyper-parameters $a_0, b_0, \alpha, \mathbf{H}$ in $\ln p(Y; a_0, b_0, \alpha, \mathbf{H})$ for simplicity.

$$\begin{aligned}
 \ln p(Y) &= \ln \left[\int \left(\prod_{d=1}^D p(\mathbf{y}_d | \boldsymbol{\theta}_d, s_d, \mathbf{f}) p(s_d) p(\boldsymbol{\theta}'_d) \right) \right. \\
 &\quad \times \left. \prod_{k=1}^{\infty} p(\mathbf{f}_{k,N} | \mathbf{f}_{k,M}) p(\mathbf{f}_{k,M}) d\boldsymbol{\theta}'_d d\mathbf{f} \right] \\
 &\geq \sum_{d=1}^D \mathbb{E} \ln p(\mathbf{y}_d | \boldsymbol{\theta}_d, s_d, \mathbf{f}) + \sum_{d=1}^D \sum_{k=1}^{K-1} \mathbb{E} \ln p(\theta'_{dk}) \\
 &\quad + \sum_{d=1}^D \mathbb{E} \ln p(s_d) + \sum_{k=1}^K \mathbb{E} \ln p(\mathbf{f}_{k,M}) \\
 &\quad - \sum_{d=1}^D \sum_{k=1}^{K-1} \mathbb{E} \ln q(\theta'_{dk}) - \sum_{d=1}^D \mathbb{E} \ln q(s_d) \\
 &\quad - \sum_{k=1}^K \mathbb{E} \ln q(\mathbf{f}_{k,M}) \triangleq \mathcal{L}_0(q). \tag{13}
 \end{aligned}$$

Because $f(\mathbf{x}) = \ln \sum_{k=1}^K \exp(x_k)$, $\mathbf{x} \in \mathbb{R}^K$ is convex, we could further bound the first term to allow for a practical variational inference. Using Jensen's inequality, we obtain

$$\begin{aligned}
 &\mathbb{E} \ln p(\mathbf{y}_d | \boldsymbol{\theta}_d, s_d, \mathbf{f}) \\
 &= \sum_{n=1}^{N_d} \left(\ln \eta_d + \mathbb{E} \ln \sum_{k=1}^{\infty} \exp(\ln \theta_{dk} + \ln f_k^2(t)) \right) \\
 &\quad - \eta_d \int_{\mathcal{T}} \mathbb{E} \sum_{k=1}^{\infty} \theta_{dk} f_k^2(s) ds \tag{14}
 \end{aligned}$$

$$\begin{aligned}
 &\geq \sum_{n=1}^{N_d} \left(\ln \eta_d + \ln \sum_{k=1}^{\infty} \exp(\mathbb{E} \ln \theta_{dk} + \mathbb{E} \ln f_k^2(t)) \right) \\
 &\quad - \eta_d \int_{\mathcal{T}} \mathbb{E} \sum_{k=1}^{\infty} \theta_{dk} f_k^2(s) ds. \tag{15}
 \end{aligned}$$

Using Equation (15), we implicitly collapse the indicator variables and obtain a lower bound of ELBO:

$$\begin{aligned}
 \mathcal{L}_1(q) &\triangleq \sum_{n=1}^{N_d} \left(\ln \eta_d + \ln \sum_{k=1}^{\infty} \exp(\mathbb{E} \ln \theta_{dk} + \mathbb{E} \ln f_k^2(t)) \right) \\
 &\quad - \eta_d \int_{\mathcal{T}} \mathbb{E} \sum_{k=1}^{\infty} \theta_{dk} f_k^2(s) ds + \sum_{d=1}^D \sum_{k=1}^{K-1} \mathbb{E} \ln \frac{p(\theta'_{dk})}{q(\theta'_{dk})} \\
 &\quad + \sum_{d=1}^D \mathbb{E} \ln \frac{p(s_d)}{q(s_d)} + \sum_{k=1}^K \mathbb{E} \ln \frac{p(\mathbf{f}_{k,M})}{q(\mathbf{f}_{k,M})}. \tag{16}
 \end{aligned}$$

Now $q(f_{k,N}) = \mathcal{N}(\tilde{u}_k, \tilde{B}_k)$, where

$$\begin{aligned}
 \tilde{u}_k &= \kappa_{k,NM} \kappa_{k,MM}^{-1} \mu_k, \\
 \tilde{B}_k &= \kappa_{k,NN} - \kappa_{k,NM} \kappa_{k,MM}^{-1} \kappa_{k,MN} \\
 &\quad + \kappa_{k,NM} \kappa_{k,MM}^{-1} \Sigma_k \kappa_{k,MM}^{-1} \kappa_{k,MN}
 \end{aligned}$$

And the expectation parts in Equation (16) can be computed as:

$$\mathbb{E} \ln p(\theta'_{dk}) = \ln \alpha + (\alpha - 1) \mathbb{E} [\ln(1 - \theta'_{dk})], \tag{17}$$

$$\begin{aligned}
 \mathbb{E} \ln q(\theta'_{dk}) &= \ln \frac{\Gamma(\tau_{dk,0} + \tau_{dk,1})}{\Gamma(\tau_{dk,0}) \Gamma(\tau_{dk,1})} \\
 &\quad + (\tau_{dk,1} - 1) \mathbb{E} [\ln(1 - \theta'_{dk})] + (\tau_{dk,0} - 1) \mathbb{E} [\ln \theta'_{dk}],
 \end{aligned} \tag{18}$$

$$\mathbb{E} \ln p(s_d) = a_0 \ln b_0 - \ln \Gamma(a_0) + (a_0 - 1) \ln \eta_d - b_0 \eta_d, \tag{19}$$

$$\begin{aligned}
 \mathbb{E} \ln \frac{p(\mathbf{f}_{k,M})}{q(\mathbf{f}_{k,M})} &= \frac{1}{2} \ln \frac{|\Sigma_k|}{|\kappa_{k,MM}|} + \frac{m}{2} \\
 &\quad - \frac{1}{2} \text{tr} \left(\kappa_{k,MM}^{-1} (\Sigma_k + (\mu_k - g)(\mu_k - g)^T) \right), \tag{20}
 \end{aligned}$$

$$\mathbb{E} [\ln f_k^2(t_n^d)] = -G \left(-\frac{\tilde{u}_{k,n}^2}{2\tilde{B}_{k,nn}} \right) - C + \ln \left(\frac{\tilde{B}_{k,nn}}{2} \right), \tag{21}$$

$$\begin{aligned}
 \int_{\mathcal{T}} \mathbb{E} [f_k^2(s)] ds &= \gamma |\mathcal{T}| - \text{tr} (\kappa_{k,MM}^{-1} \Psi_k) \\
 &\quad + \text{tr} (\kappa_{k,MM}^{-1} \Psi_k \kappa_{k,MM}^{-1} (\Sigma_k + \mu_k \mu_k^T)), \tag{22}
 \end{aligned}$$

$G(x), x \leq 0$ is calculated by a precomputed multi-resolution look-up table. C is a constant and $\Psi_k \in \mathbb{R}^{M \times M}$, $\Psi_{k,ij} = \int_{\mathcal{T}} \kappa_k(t_i, x) \kappa_k(x, t_j) dx$. Ψ_k is determined by the kernel hyper-parameter in κ_k and the region \mathcal{T} .

The expectation with regard to beta distribution is:

$$\begin{aligned}
 \mathbb{E} [\ln(1 - \theta'_{dk})] &= \psi(\tau_{dk,1}) - \psi(\tau_{dk,0} + \tau_{dk,1}), \\
 \mathbb{E} [\ln(\theta'_{dk})] &= \psi(\tau_{dk,0}) - \psi(\tau_{dk,0} + \tau_{dk,1}).
 \end{aligned}$$

After adding augmented Lagrangian penalty function,

the modified evidence lower bound is:

$$L_{\mathbf{v}_i}(\Phi, \mathbf{w}_i) \triangleq \mathcal{L}_1(q) - \sum_{k=1}^K w_{ik} \left(\int_{\mathcal{T}} \mathbb{E}_q[f_k^2(s)] ds - A \right) - \sum_{k=1}^K \frac{v_{ik}}{2} \left(\int_{\mathcal{T}} \mathbb{E}_q[f_k^2(s)] ds - A \right)^2. \quad (23)$$

A.1 Details of Derivatives

Based on the modified evidence lower bound in Equation (23), we could derive the parameter learning method.

- η_d . We list the term related to η_d in Equation (23) first.

$$L_{\eta_d} \triangleq N_d \ln \eta_d - \eta_d \int_{\mathcal{T}} \sum_{k=1}^K \mathbb{E}(\theta_{dk} f_k^2(s)) ds - \eta_d b_0 + (a_0 - 1) \ln \eta_d.$$

Obviously, there is a closed form update for η_d

$$\eta_d = \frac{N_d + a_0 - 1}{b_0 + \int_{\mathcal{T}} \sum_{k=1}^K \mathbb{E}(\theta_{dk} f_k^2(s)) ds}.$$

- $\tau_{dk,0}, \tau_{dk,1}$. We list the term related to these parameters in Equation (23) first

$$L_{\tau_{dk}} \triangleq \sum_{n=1}^{N_d} \left[\ln \sum_{k=1}^{\infty} \exp \left(\mathbb{E}_q[\ln \theta_{dk}] - \mathbb{E}_q[\ln f_k^2(t_n^d)] \right) \right] - \eta_d \int_{\mathcal{T}} \mathbb{E} \sum_{k=1}^{\infty} \theta_{dk} f_k^2(s) ds + \left(\ln \frac{\Gamma(\tau_{dk,0}) \Gamma(\tau_{dk,1})}{\Gamma(\tau_{dk,0} + \tau_{dk,1})} - (\tau_{dk,0} - 1) \mathbb{E} \ln \theta'_{dk} + (\alpha - \tau_{dk,1}) \mathbb{E} \ln(1 - \theta'_{dk}) \right).$$

Let

$$L_{dnk} \triangleq \exp \left(\mathbb{E}_q[\ln \theta_{dk}] + \mathbb{E}_q[\ln f_k^2(t_n^d)] \right) = \exp \left(\psi(\tau_{dk,0}) + \sum_{l=1}^{k-1} \psi(\tau_{dl,1}) - \sum_{l=1}^k \psi(\tau_{dl,0} + \tau_{dl,1}) + \mathbb{E}_q[\ln f_k^2(t_n^d)] \right),$$

$$V_k \triangleq \int_{\mathcal{T}} \mathbb{E} f_k^2(s) ds$$

There is no closed form update for these variables, we use coordinate ascent method.

$$\begin{aligned} \frac{\partial L_{\tau_{dk}}}{\partial \tau_{dk,0}} &= -\eta_d \left(V_k \frac{\partial[\theta_{dk}]}{\partial \tau_{dk,0}} + \sum_{l=k+1}^K V_l \frac{\partial[\theta_{dl}]}{\partial \tau_{dk,0}} \right) - \left(\tau_{dk,0} - 1 - \sum_{n=1}^{N_d} \frac{L_{dnk}}{\sum_{v=1}^K L_{dnv}} \right) \psi'(\tau_{dk,0}) \\ &+ \left(\tau_{dk,0} - 1 + \tau_{dk,1} - \alpha - \sum_{n=1}^{N_d} \frac{\sum_{v=k}^K L_{dnv}}{\sum_{v=1}^K L_{dnv}} \right) \times \psi'(\tau_{dk,0} + \tau_{dk,1}), \\ \frac{\partial L_{\tau_{dk}}}{\partial \tau_{dk,1}} &= -\eta_d \left(V_k \frac{\partial[\theta_{dk}]}{\partial \tau_{dk,1}} + \sum_{l=k+1}^K V_l \frac{\partial[\theta_{dl}]}{\partial \tau_{dk,1}} \right) - \left(\tau_{dk,1} - \alpha - \sum_{n=1}^{N_d} \frac{\sum_{v=k+1}^K L_{dnv}}{\sum_{v=1}^K L_{dnv}} \right) \psi'(\tau_{dk,1}) \\ &+ \left(\tau_{dk,0} - 1 + \tau_{dk,1} - \alpha - \sum_{n=1}^{N_d} \frac{\sum_{v=k}^K L_{dnv}}{\sum_{v=1}^K L_{dnv}} \right) \times \psi'(\tau_{dk,0} + \tau_{dk,1}), \end{aligned}$$

where we have

$$\begin{aligned} \frac{\partial[\theta_{dk}]}{\partial \tau_{dk,0}} &= \frac{\tau_{dk,1}}{(\tau_{dk,0} + \tau_{dk,1})^2} \prod_{l=1}^{k-1} \frac{\tau_{dl,1}}{\tau_{dl,0} + \tau_{dl,1}}, \\ \frac{\partial[\theta_{dk}]}{\partial \tau_{dk,1}} &= -\frac{\tau_{dk,0}}{(\tau_{dk,0} + \tau_{dk,1})^2} \prod_{l=1}^{k-1} \frac{\tau_{dl,1}}{\tau_{dl,0} + \tau_{dl,1}}, \\ \frac{\partial[\theta_{dl}]}{\partial \tau_{dk,0}} &= -\frac{\tau_{dl,0}}{\tau_{dl,0} + \tau_{dl,1}} \frac{\tau_{dk,1}}{(\tau_{dk,0} + \tau_{dk,1})^2} \\ &\times \prod_{v=1, v \neq k}^{l-1} \frac{\tau_{dv,1}}{\tau_{dv,0} + \tau_{dv,1}}, \\ \frac{\partial[\theta_{dl}]}{\partial \tau_{dk,1}} &= \frac{\tau_{dl,0}}{\tau_{dl,0} + \tau_{dl,1}} \frac{\tau_{dk,0}}{(\tau_{dk,0} + \tau_{dk,1})^2} \\ &\times \prod_{v=1, v \neq k}^{l-1} \frac{\tau_{dv,1}}{\tau_{dv,0} + \tau_{dv,1}}. \end{aligned}$$

- $\{\Sigma_k, \mu_k\}$. Take μ_k for an example.

$$\begin{aligned} \frac{\partial L_{\phi_k}}{\partial \mu_k} &= \sum_{d=1}^D \left(\sum_{n=1}^{N_d} \frac{1}{\sum_{v=1}^K L_{dnv}} \frac{\partial L_{dnk}}{\partial \mu_k} \right) - \left(w_{ik} + v_{ik} (V_k - A) + \sum_{d=1}^D \eta_d \mathbb{E}[\theta_{dk}] \right) \frac{\partial V_k}{\partial \mu_k} \\ &+ \frac{\partial}{\partial \mu_k} \left[\frac{1}{2} \ln |\Sigma_k| - \frac{1}{2} \ln |\kappa_{k,MM}| - \frac{1}{2} \text{tr} \left(\kappa_{k,MM}^{-1} (\Sigma_k + (\mu_k - g)(\mu_k - g)^T) \right) \right]. \end{aligned}$$

Hyper-parameter part: We could update the hyper-parameters in a similar way.

- Gaussian process hyper-parameters $\kappa_{k,MM}, \sigma$. Similar to that in $\{\Sigma_k, \mu_k\}$.

- Beta distribution prior α .

$$L_\alpha \triangleq D(K-1) \ln \alpha + (\alpha-1) \sum_{d=1}^D \sum_{k=1}^{K-1} (\psi(\tau_{dk,1}) - \psi(\tau_{dk,0} + \tau_{dk,1})).$$

Then we have a closed form update for α .

$$\alpha = \frac{D(K-1)}{\sum_{d=1}^D \sum_{k=1}^{K-1} (\psi(\tau_{dk,1} + \tau_{dk,0}) - \psi(\tau_{dk,1}))}. \quad (24)$$

A.2 Proof of Upper Bound

Theorem 1. *Each optimization problem is upper bounded.*

$$L_{\mathbf{v}_i}(\Phi, \mathbf{w}_i) \leq \ln p(Y) + \sum_{k=1}^K \frac{w_{ik}^2}{2v_{ik}}, \quad i \in \mathbb{N}^+.$$

lower-bounded as follows.

$$\begin{aligned} & \ln p(Y_{test} | Y_{train}; \Phi) \\ &= \ln \int p(Y_{test} | \mathbf{f}; \Phi) p(\mathbf{f} | Y_{train}; \Phi) d\mathbf{f} \\ &\approx \ln \int p(Y_{test} | \mathbf{f}; \Phi) q(\mathbf{f}; \Phi) d\mathbf{f} \\ &\geq \int q(\mathbf{f}; \Phi) \ln \frac{p(Y_{test} | \mathbf{f}; \Phi) q(\mathbf{f}; \Phi)}{q(\mathbf{f}; \Phi)} d\mathbf{f} \\ &= \mathbb{E}_q \ln p(Y_{test} | \mathbf{f}; \Phi). \end{aligned}$$

Insert the likelihood for the model and the lower bound can be further bounded as

$$\begin{aligned} & \mathbb{E}_q \ln p(Y_{test} | \mathbf{f}; \Phi) \\ &\geq \sum_{d=1}^D \sum_{n=1}^{N_d^{\text{test}}} \ln \sum_{k=1}^K \theta_{dk} \exp \left[\mathbb{E}_q (\ln f_k^2(t_n^d)) \right] \\ &\quad - \sum_{d=1}^D \sum_{k=1}^K \theta_{dk} \int_{\mathcal{T}} \mathbb{E}_q [f_k^2(s)] ds \triangleq \mathcal{L}_{test}. \end{aligned} \quad (25)$$

Proof. $\mathcal{L}_1(q)$ can be easily bounded by variational inference framework

$$\mathcal{L}_1(q) \leq \ln p(Y)$$

Let $h_{ik} = \int_{\mathcal{T}} \mathbb{E}_q [f_k^2(s)] ds - A$, and then we have

$$\begin{aligned} & \sum_{k=1}^K w_{ik} \left(\int_{\mathcal{T}} \mathbb{E}_q [f_k^2(s)] ds - A \right) \\ &+ \sum_{k=1}^K \frac{v_{ik}}{2} \left(\int_{\mathcal{T}} \mathbb{E}_q [f_k^2(s)] ds - A \right)^2 \\ &= \sum_{k=1}^K (w_{ik} h_{ik} + \frac{v_{ik}}{2} h_{ik}^2) \geq \sum_{k=1}^K \frac{w_{ik}^2}{2v_{ik}} \end{aligned}$$

Combining these two parts finishes the proof. \square

B Test Likelihood

In LPPA, the allocation matrix Θ is treated as hyper-parameters and all the parameters are $\{\boldsymbol{\mu}, \boldsymbol{\Sigma}, \mathbf{H}, \Theta\}$. Let $\Phi = \{\mathbf{H}, \Theta\}$. In variational inference we use the variational distribution $q(\mathbf{f}; \Phi)$ to approximate the posterior $p(\mathbf{f} | Y_{train}; \Phi)$. The test likelihood can be

In BaNPPA, all the parameters to be optimized are $\{\boldsymbol{\eta}, \boldsymbol{\tau}, \boldsymbol{\mu}, \boldsymbol{\Sigma}, \mathbf{H}, a_0, b_0, \alpha\}$. Let $\Phi = \{\mathbf{H}, a_0, b_0, \alpha\}$. However, if we follow the same deduction as LPPA, we will not arrive at a fair comparison since the inequality in Equation (25) is different in principle for LPPA and BaNPPA, and therefore, we draw L samples from variational distribution $q(\mathbf{s}, \boldsymbol{\theta}_d; a_0, b_0, \alpha)$ for $\mathbf{s}, \boldsymbol{\theta}_d$ and then follow the lower bound in Equation (25).

$$\begin{aligned} & \mathbb{E}_q \ln p(Y_{test} | \mathbf{s}, \boldsymbol{\Theta}, \mathbf{f}; \Phi) \\ &= \int q(\mathbf{s}, \boldsymbol{\Theta}, \mathbf{f}; \Phi) \ln p(Y_{test} | \mathbf{s}, \boldsymbol{\Theta}, \mathbf{f}; \Phi) ds d\boldsymbol{\Theta} d\mathbf{f} \\ &\approx \frac{1}{\tilde{L}} \sum_{l=1}^{\tilde{L}} \int q(\mathbf{f}; H) \ln p(Y_{test} | \mathbf{s}_l, \boldsymbol{\Theta}_l, \mathbf{f}; H) d\mathbf{f} \\ &\geq \frac{1}{\tilde{L}} \sum_{l=1}^{\tilde{L}} \left(\sum_{d=1}^D \sum_{n=1}^{N_d^{\text{test}}} \ln \left(s_{l,d} \sum_{k=1}^K \theta_{l,dk} \exp \left[\mathbb{E}_q (\ln f_k^2(t_n^d)) \right] \right) \right. \\ &\quad \left. - \sum_{d=1}^D s_{l,d} \sum_{k=1}^K \theta_{l,dk} \int_{\mathcal{T}} \mathbb{E}_q [f_k^2(s)] ds \right). \end{aligned} \quad (26)$$

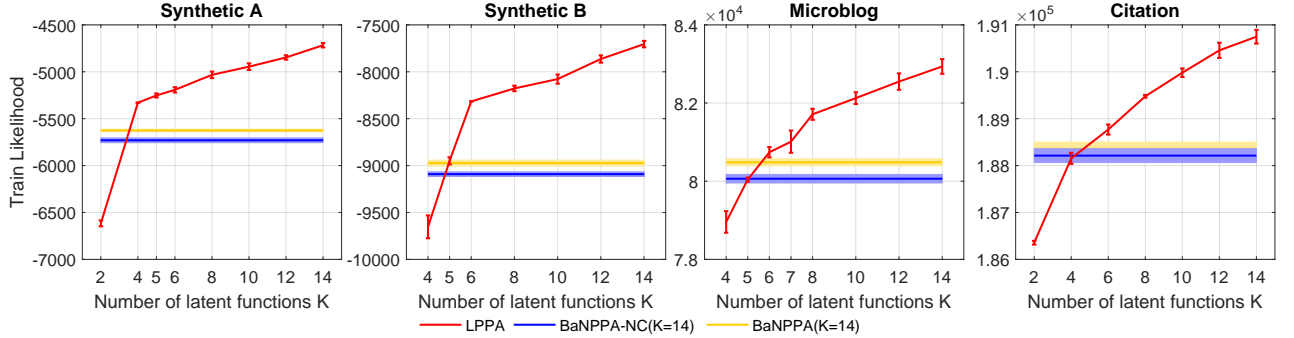


Figure 8: The comparison of the train likelihood for three algorithms. For LPPA, we change the number of latent functions K . For BaNPPA/BaNPPA-, we fix $K = 14$ and optimize the hyper-parameter α using the variational expectation-maximization. Error bars and shaded area represent the 95% confidence intervals.

C Additional Experiment Results

C.1 Details of the Data Sets

- **Synthetic dataset.**

A) In $\lambda_d(t) = s_d \sum_{k=1}^4 \theta_{dk} \tilde{f}(t; \psi_k)$, $t \in [0, 60]$.

$$s_d \sim \text{Gamma}(2, 3),$$

$$\theta_d \sim \text{Dirichlet}(1.2, 1, 0.8, 0.6),$$

$$\begin{aligned} \tilde{f}(t; \psi_k) \propto & \exp\left(-\frac{(t-15+10k)^2}{10}\right) \\ & + \exp\left(-\frac{(t-55+10k)^2}{10}\right). \end{aligned}$$

Each $\tilde{f}(t; \psi_k)$ is either a Gaussian distribution or a mixture of two Gaussian distributions normalized by its integral.

B) In $\lambda_d(t) = s_d \sum_{k=1}^6 \theta_{dk} f_k(t)$.

$$s_d \sim \text{Gamma}(2, 3),$$

$$\theta_d \sim \text{Dirichlet}(1.2, 1, 0.8, 0.6, 0.5, 0.5),$$

$$\begin{aligned} \tilde{f}(t; \psi_k) \propto & \exp\left(-\frac{(t-15+10k)^2}{10}\right) \\ & + \exp\left(-\frac{(t-75+10k)^2}{10}\right). \end{aligned}$$

Each $\tilde{f}(t; \psi_k)$ is either a Gaussian distribution or a mixture of two Gaussian distributions normalized by its integral. We use the rejection sampling method for the inhomogeneous Poisson process to generate the time sequences.

- **citation dataset.** Two examples with different citation patterns are given in Figure 9.

C.2 The Comparison of the Train Likelihood

The comparison of the train likelihood \mathcal{L}_{train} is given in Figure 8. We can notice that for LPPA, the train

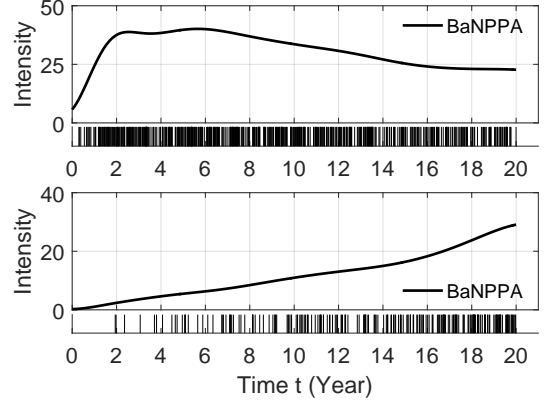


Figure 9: **Citation data set.** Top: A paper which slowly gets citation and becomes popular many years later. Bottom: A paper which quickly gets citation after being published. Smooth lines are the mean intensity function inferred from LPPA and BaNPPA. Small bars are the time of each citation. The x-axis indicates the time in year after publication.

likelihood keeps increasing when we increase K . This is also a sign of over-fitting.

C.3 Computation Time

We plot the change of the training likelihood in one trial in Figure 10. For total computational complexity, both BaNPPA- and BaNPPA take more computation time but are still comparable to LPPA. Two reasons account for this fact. One is that there are more parameters to be optimized in BaNPPA and BaNPPA- and the other is that BaNPPA potentially has an infinite number of problems to be solved. In Figure 10, we can notice that the training likelihood for BaNPPA and the training likelihood for BaNPPA- stabilize rather quickly. This is because we use Equa-

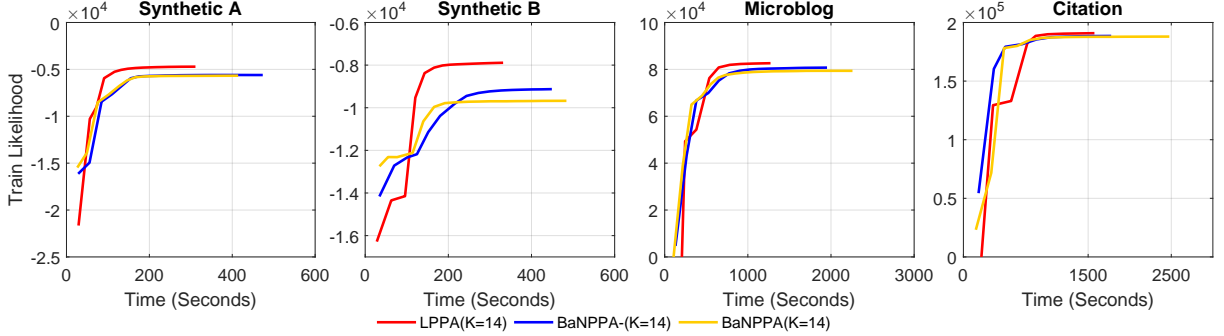


Figure 10: The comparison of the training likelihood versus time for four data sets ($K=14$) when optimizing the hyper-parameter α . The result of one trial is shown.

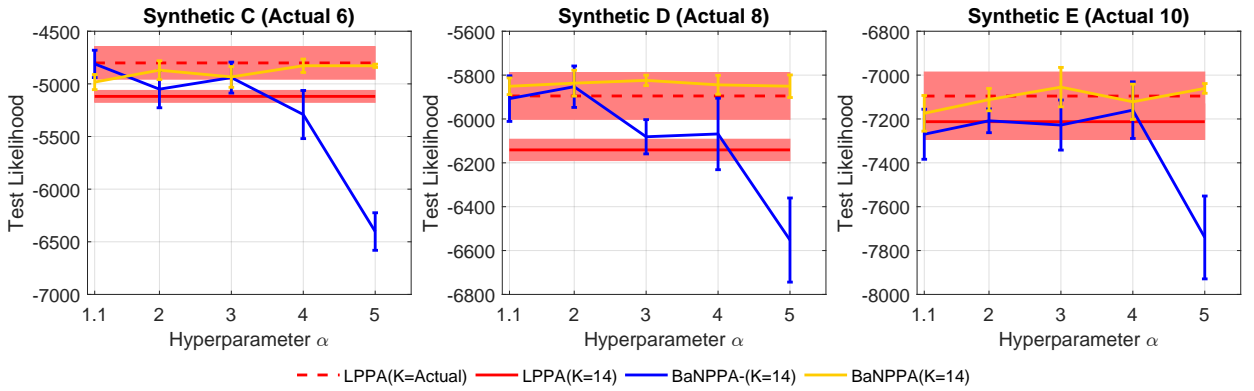


Figure 11: The comparison of the test likelihood for three additional data sets ($K=14$) when fixing the hyper-parameter $\alpha = [1.1, 2, 4, 6, 8]$. Error bars and shaded area represent the 95% confidence intervals.

tion (26) to calculate the likelihood and there are no divergence terms in it.

C.4 Synthetic Data Sets with a Relatively Large K

We add three more synthetic data set with a larger K .

C) We sample 200 sequences from $\lambda_d(t) = s_d \sum_{k=1}^6 \theta_{dk} \tilde{f}(t; \psi_k)$, where s_d , θ_d are drawn from Dirichlet distribution and Gamma distribution.

$$s_d \sim \text{Gamma}(2, 3),$$

$$\theta_d \sim \text{Dir}(0.8, 0.4, 0.2, 0.2, 0.2, 0.2).$$

We use $\tilde{f}(t; \psi_k) = \exp(-(t - 15 + 10k)^2/10)$, $k = 1, \dots, 6$, $t \in [0, 60]$ as basis intensity functions.

D) We sample 200 sequences from $\lambda_d(t) = s_d \sum_{k=1}^8 \tilde{f}(t; \psi_k)$, where s_d , θ_d are drawn from Dirichlet distribution and Gamma distribution.

$$s_d \sim \text{Gamma}(2, 3),$$

$$\theta_d \sim \text{Dir}(0.8, 0.4, 0.4, 0.2, 0.2, 0.2, 0.1, 0.1).$$

We use $\tilde{f}(t; \psi_k) \propto \exp(-(t - 15 + 10k)^2/10)$, $k = 1, \dots, 8$, $t \in [0, 80]$ as basis intensity functions.

E) We sample 200 sequences from $\lambda_d(t) = s_d \sum_{k=1}^{10} \tilde{f}(t; \psi_k)$, where s_d , θ_d are drawn from Dirichlet distribution and Gamma distribution.

$$s_d \sim \text{Gamma}(2, 3),$$

$$\theta_d \sim \text{Dir}(0.8, 0.6, 0.4, 0.4, 0.4, 0.2, 0.2, 0.2, 0.1, 0.1).$$

We use $\tilde{f}(t; \psi_k) \propto \exp(-(t - 15 + 10k)^2/10)$, $k = 1, \dots, 10$, $t \in [0, 100]$ as basis intensity functions.

In the experiment, we fix the hyper-parameter a_0 and b_0 and the length-scale hyper-parameters in all $\kappa_{k,MM}$ to be 4.3081 (Close to the half of the span of $\tilde{f}(t; \psi_k)$). This means we only optimize the mixture weights and the variational distribution $q(m, S)$ for Gaussian processes.

We vary the hyper-parameter $\alpha = [1.1, 2, 3, 4, 5]$. The result is given in Figure. We can see that BaNPPA tends to over-shrink the components even when $\alpha = 5$ and gets a worse result.

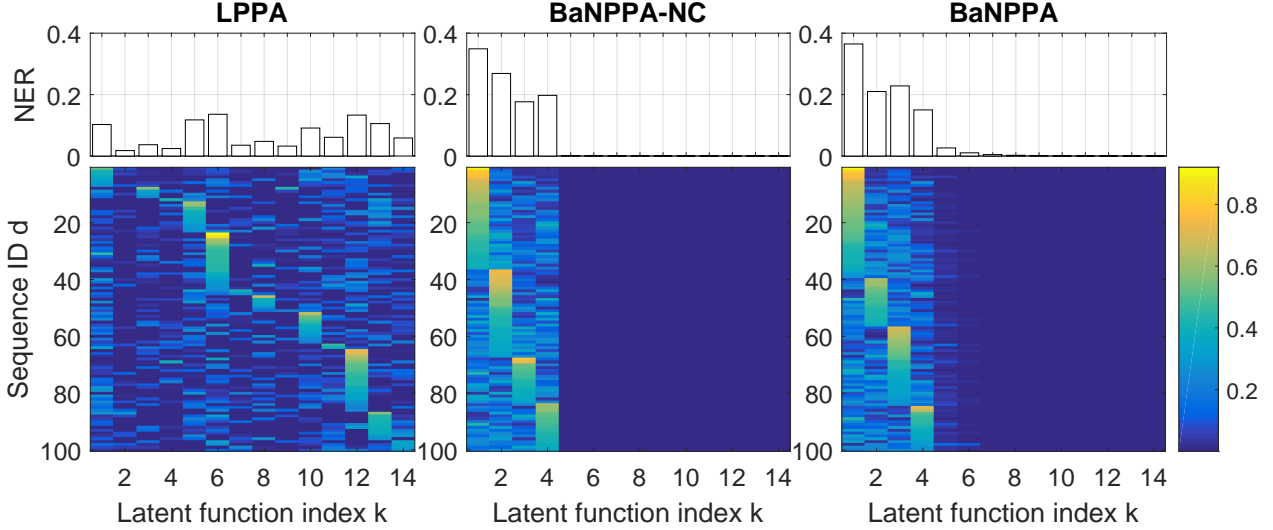


Figure 12: **Synthetic A data set.** Comparisons of the matrix $\hat{\Theta}$ among LPPA (Left), BaNPPA-NC (middle) and BaNPPA (Right) when optimizing α . $K = 14$. The result of the trial with the best test likelihood is given.

C.5 The Comparison of Three algorithms on Four Data Sets Using $\hat{\Theta}$

On the four data sets, we plot the normalized allocation matrix $\hat{\Theta}$ in the trial with the best test likelihood. We sample 100 time-sequences (125 in the Synthetic B data set) from each data set. We reorder the ID of the time-sequences: first by the index of the largest element $c_d = \arg \max_k \theta_{dk}$ (e.g., group all time-sequences whose $c_d = 1$ together), and then by the value of the largest element $\max_k \theta_{dk}$. The comparison for LPPA, BaNPPA-NC and BaNPPA is given from Figure 12 to 15. We can notice that LPPA tends to utilize all latent functions and BaNPPA-NC tends to over-shrink the additional latent functions and present sharp results.

References

R. P. Adams, I. Murray, and D. J. MacKay. Tractable nonparametric bayesian inference in poisson processes with gaussian process intensities. In *Proceedings of the 26th Annual International Conference on Machine Learning*, pages 9–16. ACM, 2009.

M. Bauer, M. van der Wilk, and C. E. Rasmussen. Understanding probabilistic sparse gaussian process approximations. In *Advances in Neural Information Processing Systems*, pages 1533–1541, 2016.

D. P. Bertsekas. *Constrained optimization and Lagrange multiplier methods*. Academic press, 2014.

D. M. Blei, M. I. Jordan, et al. Variational inference for dirichlet process mixtures. *Bayesian analysis*, 1(1):121–143, 2006.

S. Gao, J. Ma, and Z. Chen. Modeling and predicting retweeting dynamics on microblogging platforms. In *Proceedings of the Eighth ACM International Conference on Web Search and Data Mining*, pages 107–116. ACM, 2015.

P. Gopalan, F. J. Ruiz, R. Ranganath, and D. Blei. Bayesian nonparametric poisson factorization for recommendation systems. In *Artificial Intelligence and Statistics*, pages 275–283, 2014.

T. Gunter, C. Lloyd, M. A. Osborne, and S. J. Roberts. Efficient bayesian nonparametric modelling of structured point processes. In *Proceedings of the Thirtieth Conference on Uncertainty in Artificial Intelligence*, pages 310–319. AUAI Press, 2014.

J. Hensman, N. Fusi, and N. D. Lawrence. Gaussian processes for big data. In *Proceedings of the Twenty-Ninth Conference on Uncertainty in Artificial Intelligence*, pages 282–290. AUAI Press, 2013.

A. T. Ihler and P. Smyth. Learning time-intensity profiles of human activity using non-parametric bayesian models. In *Advances in Neural Information Processing Systems*, pages 625–632, 2007.

J. F. C. Kingman. *Poisson processes*. Wiley Online Library, 1993.

A. Kottas. Dirichlet process mixtures of beta distributions, with applications to density and intensity estimation. In *Workshop on Learning with Nonparametric Bayesian Methods, 23rd International Conference on Machine Learning (ICML)*, 2006.

W. Lian, R. Henao, V. Rao, J. Lucas, and L. Carin. A multitask point process predictive model. In *Proceedings of the 32nd International Conference*

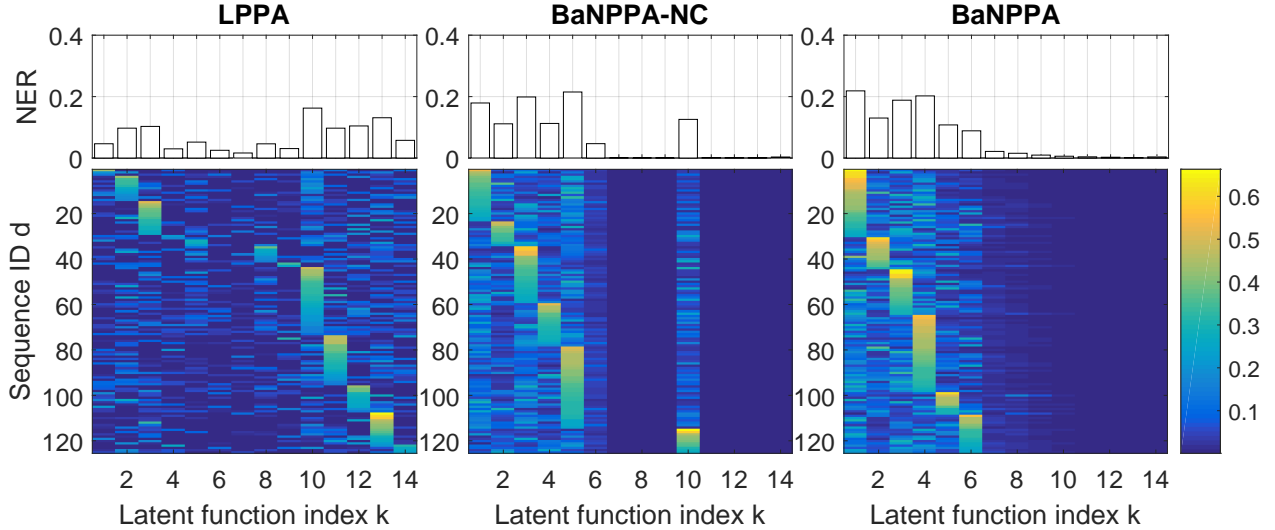


Figure 13: **Synthetic B data set.** Comparisons of the matrix $\hat{\Theta}$ among LPPA (Left), BaNPPA-NC (middle) and BaNPPA (Right) when optimizing α . $K = 14$. The result of the trial with the best test likelihood is given.

on Machine Learning (ICML-15), pages 2030–2038, 2015.

H. Liu and D. E. Brown. Criminal incident prediction using a point-pattern-based density model. *International journal of forecasting*, 19(4):603–622, 2003.

C. Lloyd, T. Gunter, M. Osborne, and S. Roberts. Variational inference for gaussian process modulated poisson processes. In *International Conference on Machine Learning*, pages 1814–1822, 2015.

C. Lloyd, T. Gunter, M. Osborne, S. Roberts, and T. Nickson. Latent point process allocation. In *Artificial Intelligence and Statistics*, pages 389–397, 2016.

A. Miller, L. Bornn, R. Adams, and K. Goldsberry. Factorized point process intensities: A spatial analysis of professional basketball. In *International Conference on Machine Learning*, pages 235–243, 2014.

J. Pitman, N. M. Tran, et al. Size-biased permutation of a finite sequence with independent and identically distributed terms. *Bernoulli*, 21(4):2484–2512, 2015.

M. Schmidt, E. Berg, M. Friedlander, and K. Murphy. Optimizing costly functions with simple constraints: A limited-memory projected quasi-newton algorithm. In *Artificial Intelligence and Statistics*, pages 456–463, 2009.

Y. W. Teh, M. I. Jordan, M. J. Beal, and D. M. Blei. Sharing clusters among related groups: Hierarchical dirichlet processes. In *Advances in neural information processing systems*, pages 1385–1392, 2005.

M. K. Titsias. Variational learning of inducing variables in sparse gaussian processes. In *AISTATS*, volume 5, pages 567–574, 2009.

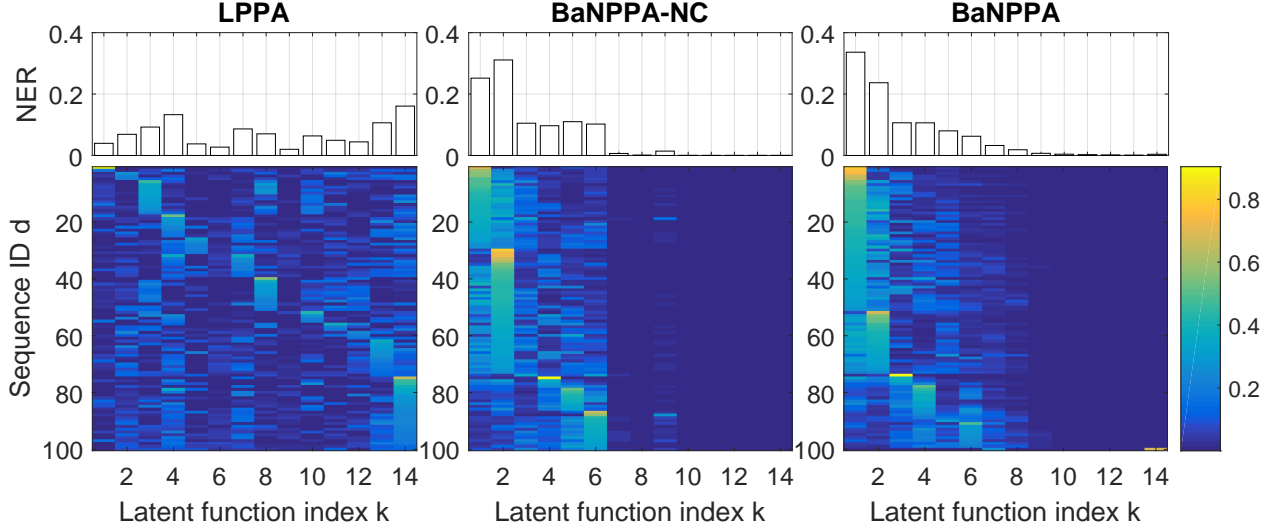


Figure 14: **Microblog data set.** Comparisons of the matrix $\hat{\Theta}$ among LPPA (Left), BaNPPA-NC (middle) and BaNPPA (Right) when optimizing α . $K = 14$. The result of the trial with the best test likelihood is given.

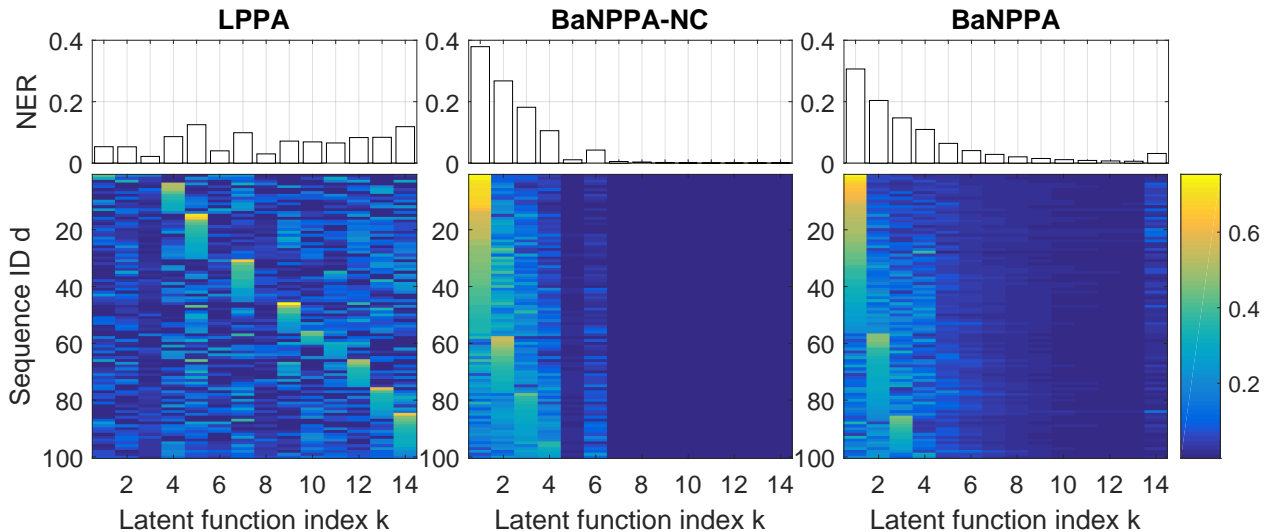


Figure 15: **Citation data set.** Comparisons of the matrix $\hat{\Theta}$ among LPPA (Left), BaNPPA-NC (middle) and BaNPPA (Right) when optimizing α . $K = 14$. The result of the trial with the best test likelihood is given.